Rapid Communications

Giant anisotropic magnetoresistance and planar Hall effect in the Dirac semimetal Cd_3As_2

Hui Li,[1] Huan-Wen Wang,[2] Hongtao He,[3] Jiannong Wang,[1,*] and Shun-Qing Shen[2,†]

[1]*Department of Physics, the Hong Kong University of Science and Technology, Clear Water Bay, Hong Kong, China*
[2]*Department of Physics, the University of Hong Kong, Pokfulam Road, Hong Kong, China*
[3]*Department of Physics, Southern University of Science and Technology, Shenzhen, Guangdong 518055, China*

(Received 9 March 2018; revised manuscript received 30 April 2018; published 14 May 2018)

Anisotropic magnetoresistance is the change tendency of resistance of a material on the mutual orientation of the electric current and the external magnetic field. Here, we report experimental observations in the Dirac semimetal Cd_3As_2 of giant anisotropic magnetoresistance and its transverse version, called the planar Hall effect. The relative anisotropic magnetoresistance is negative and up to −68% at 2 K and 10 T. The high anisotropy and the minus sign in this isotropic and nonmagnetic material are attributed to a field-dependent current along the magnetic field, which may be induced by the Berry curvature of the band structure. This observation not only reveals unusual physical phenomena in Weyl and Dirac semimetals, but also finds additional transport signatures of Weyl and Dirac fermions other than negative magnetoresistance.

DOI: 10.1103/PhysRevB.97.201110

Anisotropic magnetoresistance (AMR) was first discovered by Thomson in 1857 and was observed in many ferromagnetic metals [1]. It is closely associated with changes of magnetization relative to the current. Its transverse version shows a transverse current or voltage in response to the longitudinal current flow and an applied in-plane magnetic field, called the planar Hall effect (PHE) [2,3]. Usually, the relative AMR is weak, less than 1% or at most up to a few percent in some ferromagnetic metals and half-metallic ferromagnets [4]. Recently, negative longitudinal magnetoresistance and nonsaturated linear out-of-plane perpendicular magnetoresistance and in-plane transverse magnetoresistance were reported in a series of newly discovered topological semimetals [5–16]. While negative magnetoresistance is possibly associated with the chiral anomaly of the Weyl fermions in an electric field and a magnetic field [17–20], linear out-of-plane perpendicular magnetoresistance and in-plane transverse magnetoresistance illustrate the high anisotropy of magnetotransport in topological semimetals. This is a rare property for a paramagnetic metal. The AMR and PHE have started to attract a lot of theoretical studies in topological semimetals [21,22] and other topological materials [23–25].

We denote transverse resistivity by $\rho_\perp(B)$ when the magnetic field $\mathbf{B}$ is perpendicular to the electric current density $\mathbf{j}$, i.e., $\mathbf{j}\cdot\mathbf{B}=0$, and longitudinal resistivity by $\rho_\parallel(B)$ when the magnetic field is parallel to the electric current density, i.e., $\mathbf{B}\parallel\mathbf{j}$. Usually, transverse resistivity is larger than longitudinal resistivity, i.e., $\rho_\perp(B)\geqslant\rho_\parallel(B)$, in Weyl and Dirac semimetals. The equality holds only for $B=0$. Thus, the resistivity is very sensitive to the angle between the electric current density and the magnetic field. In general, the AMR and PHE can be well described by a formula between the electric field $\mathbf{E}$ and the electric current density in a vector form as below,

$$\mathbf{E}=\rho_\perp\mathbf{j}+(\rho_\parallel-\rho_\perp)\frac{\mathbf{B}\mathbf{B}\cdot\mathbf{j}}{B^2}+\rho_\perp\chi\mathbf{B}\times\mathbf{j}, \tag{1}$$

where χ is the mobility of the charge carriers. Assuming $\mathbf{j}$ and $\mathbf{B}$ construct an $x-y$ plane [see Fig. 1(a)], the in-plane field-dependent resistivity $\rho_{ij}=\rho_\perp\delta_{ij}+(\rho_\parallel-\rho_\perp)B_iB_j/B^2$, with $i,j=x,y$. In-plane diagonal or longitudinal resistivity is highly anisotropic as a function of the angle φ between the magnetic field and electric current density, $\rho_{xx}=\frac{\rho_\parallel+\rho_\perp}{2}+\frac{\rho_\parallel-\rho_\perp}{2}\cos 2\varphi$. In-plane off-diagonal resistivity leads to a nonzero electric field that is normal to the electric current density but parallel to the magnetic field. In-plane off-diagonal resistivity is called planar Hall resistivity, $\rho_{xy}=\frac{\rho_\parallel-\rho_\perp}{2}\sin 2\varphi$. It is worth emphasizing that $\rho_{xx}(\varphi)$ and $\rho_{xy}(\varphi)$ have identical forms to that for ferromagnetic metals [1].

In our previous magnetotransport study of Dirac semimetal Cd_3As_2 microribbons [8], we have successfully observed the carrier density dependence of nonsaturating positive magnetoresistance in out-of-plane perpendicular magnetic fields and negative longitudinal magnetoresistance in parallel magnetic fields. Here, we present further in-plane magnetotransport results on the AMR and PHE in Dirac semimetal Cd_3As_2 microribbons. Our experimental results are in excellent agreement with the relation between the magnetic field and electric current density in Eq. (1), which can be derived from the field-dependent current induced by the chiral anomaly of Weyl and Dirac fermions, or the Berry curvature in conventional and topological metals in the semiclassical theory. This implies that the observed AMR and PHE in our Cd_3As_2 microribbons is associated with the physics of Berry curvature intrinsic to the Dirac semimetal Cd_3As_2.

Detailed growth and structural charaterizations of Cd_3As_2 microribbons can be found in our earlier work [8]. In brief, a Cd_3As_2 microribbon was grown by the chemical vapor deposition method on Si (001) substrates and Ar gas was used as a carrier gas. The furnace was gradually heated up to

*Authors to whom correspondence and requests for materials should be addressed: phjwang@ust.hk
†sshen@hku.hk

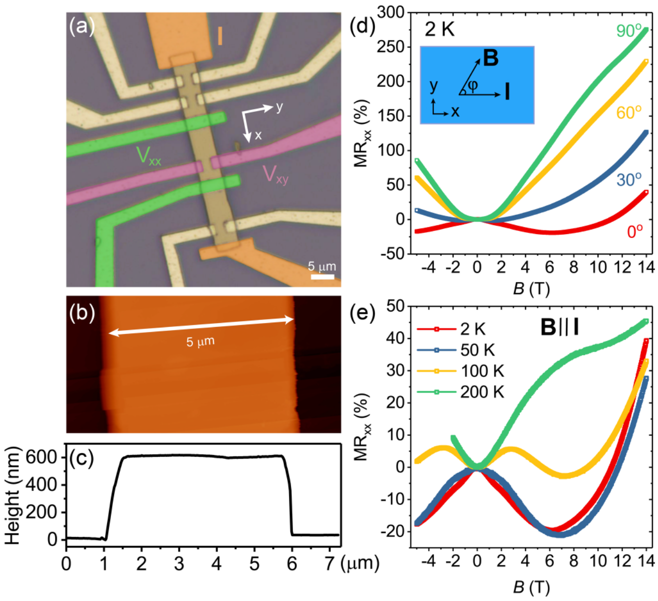

FIG. 1. Cd_3As_2 microribbon devices and magnetotransport characteristics. (a) The optical image of the Cd_3As_2 microribbon device. The current probes **I** and voltage probes V_{xx} and V_{xy} are labeled in orange, green, and purple colors, respectively. The current is applied along the x direction as indicated, and the microribbon is rotated in the $x-y$ plane. (b) AFM image and (c) the height profile of the Cd_3As_2 microribbon in (a). (d) The in-plane longitudinal magnetoresistance (MR_{xx}) measured at 2 K with the applied magnetic field (**B**) direction changing from parallel ($\varphi = 0^\circ$) to transverse ($\varphi = 90^\circ$) to the applied current (**I**) direction in the $x-y$ plane. (e) In-plane longitudinal magnetoresistance (MR_{xx}) measured at the different temperatures indicated in parallel fields in the $x-y$ plane.

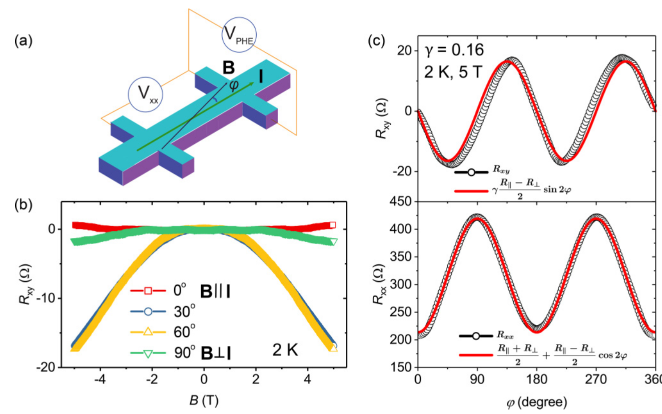

FIG. 2. Planar Hall effect (PHE) in the Cd_3As_2 microribbon. (a) Schematic of the PHE in the Cd_3As_2 microribbon devices. (b) The magnetic field dependence of the R_{xy} measured at 2 K with the applied **B**-field direction changing from parallel ($\varphi = 0^\circ$) to transverse ($\varphi = 90^\circ$) to the applied current direction in the $x-y$ plane. (c) The symmetrized angular dependence of the R_{xy} (top panel) and R_{xx} (bottom panel) measured at 2 K and 5 T. The red lines are the fitting curves using the inset equations, where φ is the angle between the **I** and **B** field in the $x-y$ plane; $R_\parallel$ and $R_\perp$ are the resistance when φ is equal to 0° and 90°, respectively; γ is the ratio of the width to the length of the Cd_3As_2 microribbon device.

750 °C in 20 min and the Ar flow was kept as 100 sccm (sccm denotes cubic centimeter per minute at standard temperature and pressure) during the growth process. The duration of the growth is 60 min, and then it cools down to room temperature naturally. To study the magnetotransport properties, a Hall bar structure was fabricated with standard e-beam lithography and lift-off processes. Al/Au/Cr electrodes with thicknesses of 500 nm/175 nm/25 nm were deposited using thermal evaporation and e-beam evaporation methods. The transport properties of the devices were then measured in a Quantum Design physical properties measurement system (PPMS) with the highest magnetic field up to 14 T.

Figure 1(a) shows the optical image of a typical Cd_3As_2 device studied in this work. The width w is about 5 μm, and the intervoltage-probe distance for V_{xx} and V_{xy} is about 10 and 2 μm, respectively. The ribbon thickness t is about 592 nm according to the atomic force microscopy measurement shown in Fig. 1(b) and the measured height profile in Fig. 1(c). The current **I** is applied along the longitudinal direction (x direction) of the Cd_3As_2 microribbon, as indicated in Fig. 1(a). The carrier concentration and mobility is in the order of $10^{17}/\text{cm}^3$ and $10^4\,\text{cm}^2/\text{V s}$, respectively, for temperatures below 50 K. The Fermi energy E_F, defined as the energy difference between the Fermi level and the Dirac point, is estimated to be about 88 meV above the Dirac point based on the known Fermi velocity $v_F \sim 10^6$ m/s for Cd_3As_2 [26] (see Sec. A in the Supplemental Material [27] for details). Figure 1(d) shows the in-plane longitudinal magentoresistance ($MR_{xx} = \frac{R_{xx}(B)-R_{xx}(0)}{R_{xx}(0)} \times 100\%$) measured at $T = 2$ K with various angles φ between the applied magnetic field and current directions in the $x-y$ plane (see the inset). When the magnetic field (**B** field) is parallel to the applied current (**I**), i.e., $\varphi = 0^\circ$, a pronounced negative MR_{xx} is observed in low magnetic fields. When φ increases, negative MR_{xx} vanishes and an evident positive MR_{xx} is observed. It reaches the maximum value of $\sim$275% at 14 T when the **B** field is transverse to **I** ($\varphi = 90^\circ$). Figure 1(e) shows the MR_{xx} curves measured at $\varphi = 0^\circ$ at the indicated temperatures. Negative MR_{xx} has been observed in a wide temperature range, and the largest negative MR_{xx} of $\sim -21\%$ is observed at $T = 50$ K and $B = 7$ T. However, negative MR_{xx} is not observable when the temperature further increases to above 200 K. Similar MR_{xx} behaviors have been observed in other Cd_3As_2 microribbon devices. Such negative MR_{xx} has been studied in detail and attributed to the chiral anomaly in our previous work [8]. Similar observations of negative MR_{xx} with $\mathbf{B} \parallel \mathbf{I}$ have also been reported and are considered as a signature of the chiral anomaly of topological semimetals [5–7,9–12].

According to Eq. (1), the longitudinal resistance (diagonal) R_{xx} and the planar Hall resistance (off-diagonal) R_{xy}, defined as $R_{xy} = \frac{V_{xy}}{I}$, change systematically as a function of the rotating angle φ. Figure 2(a) is a schematic illustration of the PHE in the Cd_3As_2 microribbon devices, the current **I** is applied along the longitudinal direction of the Cd_3As_2 microribbon, and the **B** field is rotated in the $x-y$ plane. In the experiment, a misalignment between the actual rotation plane and the Cd_3As_2 microribbon plane may exist. This could result in a finite ordinary Hall resistivity component in the measured planar Hall resistivity R_{xy}. Fortunately, the ordinary

Hall component is antisymmetric to the **B**-field directions and can be readily eliminated by summing the measured R_{xy} in both positive and negative **B**-field directions. Figure 2(b) shows the symmetrized **B**-field dependence of the R_{xy} measured at different rotating angles φ at 2 K. When φ varies from 0° to 90°, the magnitude of R_{xy} increases first and then decreases, as expected in the PHE discussions of Eq. (1).

Figure 2(c) shows the symmetrized angular-dependent R_{xy} and R_{xx} measured at 2 K and 5 T. Both the measured R_{xy} and R_{xx} show a 180° periodic angular dependence, which is not expected for a nonmagnetic and isotropic solid but is in agreement with Eq. (1). We fit the R_{xy} using the equation $R_{xy} = \gamma \frac{R_\parallel - R_\perp}{2} \sin 2\varphi$ derived from Eq. (1), where $R_\parallel$ and $R_\perp$ is the longitudinal resistance when φ is equal to 0° and 90°, respectively, and γ is the geometric ratio of the width to the length of the Hall bar device. Remarkably, as indicated by the red line in the top panel in Fig. 2(c), the measured R_{xy} can be well fitted by the equation, demonstrating the existence of the PHE in this nonmagnetic material. Moreover, the measured R_{xx} can also be well fitted by the equation $R_{xx}(B,\varphi) = \frac{R_\parallel + R_\perp}{2} + \frac{R_\parallel - R_\perp}{2} \cos 2\varphi$, as indicated by the red line in the bottom panel in Fig. 2(c). Such a periodic resistance oscillation is a peculiar characteristic of the AMR, as will be discussed below. The same PHE and AMR features have been observed in other Cd_3As_2 microribbon devices, as can be seen in Sec. B in the Supplemental Material [27].

Prior to discussing the AMR effect, we revisit the $R_{xx}-\mathbf{B}$ curves at different rotating angles φ, as shown in Fig. 3(a). According to Eq. (1), the longitudinal resistance R_{xx} follows $R_{xx}(B,\varphi)$. Theoretically, we can calculate the R_{xx} value at any arbitrary angle φ if the R_{xx} values at $\varphi = 0°$ ($R_\parallel$) and 90° ($R_\perp$) are known. As shown in Fig. 3(a), the measured $R_{xx}-\mathbf{B}$ curves at $\varphi = 0°$, 30°, 60°, and 90° in a magnetic field range of ±5 T are plotted. The red lines are the calculated results of $R_{xx}(B,\varphi)$ using the measured curves at $\varphi = 0°$ and 90°. The yielded φ is 27° and 55°, respectively, which is very close to the experimental set values of 30° and 60°. The difference may be caused by the misalignment between the actual rotation plane and the Cd_3As_2 microribbon plane. Figure 3(b) shows the symmetrized angular-dependent R_{xx} at the **B** fields indicated and 2 K. The AMR effect can be seen clearly at different **B** fields and can be well described by $R_{xx}(B,\varphi)$ [red lines in Fig. 3(b)].

More remarkably, the observed AMR here shows anomalously larger $R_\perp$ than $R_\parallel$. Thus, the AMR ratio, defined as $\frac{R_\parallel - R_\perp}{R_\perp} \times 100\%$ [4], is negative for the Cd_3As_2 microribbon device at 2 K, as shown in Fig. 3(c). With increasing **B** fields, the magnitude of the AMR ratio increases monotonically and saturates at ~68% around $B = 10$ T. In Fig. 3(c), indicated as solid symbols, the saturated AMR ratios for ferromagnetic metals CoMnAl, NiFe, and Fe_4N and half-metallic ferromagnet $La_{0.7}Sr_{0.3}MnO_3$ are replotted from Ref. [4] for comparison. As can be seen, the saturated AMR ratio for the Cd_3As_2 microribbon device is one or two orders of magnitude larger than that for ordinary ferromagnetic metals and half-metallic ferromagnets. This giant and negative AMR is a striking feature in topological Weyl and Dirac semimetals. Moreover, the AMR amplitude follows a quadratic **B**-field dependence at a small **B**-field regime ($B < 1.0$ T), as theoretically expected (see Sec. C in the Supplemental Material [27] for details). However, the AMR amplitude deviates from the quadratic function at a higher **B** field above 3.5 T, which may be caused for multiple reasons and is still under theoretical investigation.

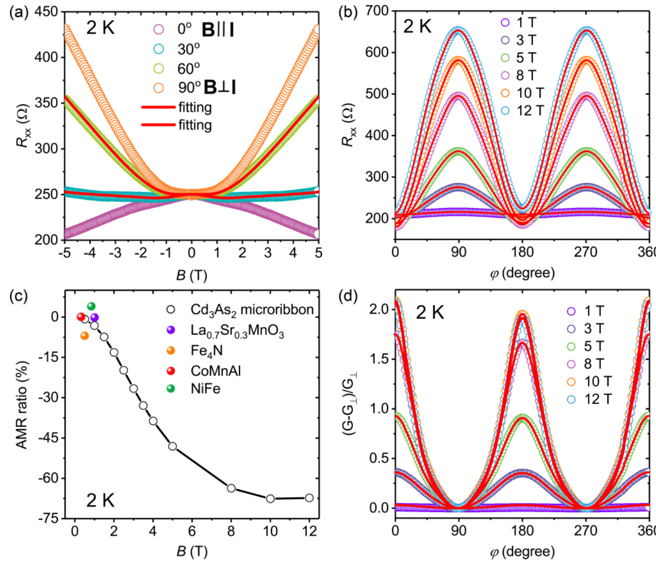

FIG. 3. Anisotropic magnetoresistance (AMR) in the Cd_3As_2 microribbon. (a) The symmetrized longitudinal resistance (R_{xx}) measured at 2 K at φ indicated, where φ is the angle between the **I** and **B** field in the $x-y$ plane. (b) The angular dependence of the R_{xx} at 2 K and **B** fields indicated. The red lines in (a) and (b) are fitting curves using $R_{xx} = \frac{R_\parallel + R_\perp}{2} + \frac{R_\parallel - R_\perp}{2} \cos 2\varphi$. (c) The AMR ratio of the Cd_3As_2 microribbon devices at 2 K as a function of the **B** fields. The black line is a guide to the eyes. The AMR ratio of ferromagnetic metals CoMnAl, NiFe, Fe_4N, and half-metallic ferromagnet $La_{0.7}Sr_{0.3}MnO_3$ from Ref. [23] is also indicated for comparison. (d) The angular dependence of the in-plane longitudinal conductance G_{xx} at 2 K and **B** fields indicated. The red lines are the fitting curves using Eq. (3).

Figure 3(d) shows the angular-dependent magnetoconductance. The longitudinal magnetoconductance is not simply proportional to $\cos^2\varphi$. The nonsinusoidal feature becomes more evident when increasing the **B** field from 1 to 10 T, demonstrating that the measured AMR increased with the magnetic field. This effect can be well understood from the AMR and PHE [21]. In this case, the conductance G is given as R^{-1}, and the relative longitudinal magnetoconductance is then given by

$$\frac{G - G_\perp}{G_\perp} = \frac{\cos^2\varphi}{\frac{R_\parallel}{R_\perp - R_\parallel} + \sin^2\varphi}. \tag{2}$$

The correction of $\sin^2\varphi$ in the denominator reflects the in-plane transverse voltage induced by the applied **B** field or the PHE. This is another peculiar feature of the AMR. We plug the experimental value of $R_\parallel$ and $R_\perp$ into Eq. (2) to reproduce the angular-dependent magnetoconductance [red lines in Fig. 3(d)], which shows very good agreement with the experimentally measured ones [open circles in Fig. 3(d)]. Thus the PHE is attributed to this angle narrowing effect. This angle narrowing effect was also observed in a previous experiment [6], which implies the existence of PHE in Na_3Bi.

The AMR and PHE can be attributed to a **B**-field-dependent current given by

$$\mathbf{j}_{\mathrm{B}} = \alpha(\mathbf{B}\cdot\mathbf{E})\mathbf{B}. \tag{3}$$

The key feature of Eq. (3) is that the current density is parallel to the magnetic field instead of the electric field. Several mechanisms may produce this type of current: (1) The chiral magnetic effect of Weyl fermions gives a nonzero current density which is proportional to the magnetic field **B**, $\mathbf{j}_{\mathrm{CME}} = \frac{e^2}{4\pi^2\hbar^2}\mu_5\mathbf{B}$, where μ_5 is the chemical potential difference between the two Weyl nodes according to the quantum field theory [28,29]. However, when the Weyl fermions are subject to both an electric field **E** and a magnetic field **B**, the chiral anomaly equations for Weyl fermions induce a nonzero value $\mu_5 \approx \frac{e^2\hbar v_F^3\mathbf{E}\cdot\mathbf{B}\tau_v}{\mu^2}$, where τ_v is the relaxation time, v_F is the Fermi velocity, and μ is the chemical potential. Substituting μ_5 into the current equation of the chiral magnetic effect, one obtains $\alpha = \frac{e^2}{4\pi^2\hbar}\frac{e^2v^3\tau_v}{\mu^2}$. α is anticipated to be a constant in weak magnetic fields [18] and become field dependent at strong fields [30]. (2) In the second-order semiclassical theory [31], the Berry curvature in a conventional metal without chiral anomaly can also produce a current along the direction of the **B** field. It is attributed to the Fermi surface property that highly depends on the geometric quantities such as the orbital magnetic moment. For nonmagnetic metals in the semiclassical regime, the leading-order magnetoresistivity is quadratic of B due to the constraint of time-reversal symmetry and the Onsager's relation [32]. (3) Other possible mechanisms are also proposed in conventional and topological conductors. For example, the electric and magnetic field can produce a helicity imbalance leading to the field-dependent current in a Dirac-like material [33].

In the presence of a magnetic field, the Lorentz force, which deflects the motion of charged particles in a magnetic field, is also one of the main sources to produce magnetotransport in a solid. Considering the drift velocity of charge carriers in a magnetic field and the field-dependent correction to the charge current, the charge current density **j** can be expressed as

$$\mathbf{j} - \chi\mathbf{j}\times\mathbf{B} = \sigma_D\mathbf{E} + \alpha(\mathbf{E}\cdot\mathbf{B})\mathbf{B}, \tag{4}$$

where σ_D is the isotropic conductivity, and χ is the mobility. The resulting resistivity is a tensor instead of a scalar after $\mathbf{j}_{\mathrm{B}}$ is included. When the magnetic field is transverse to the electric current density, i.e., $\mathbf{j}\cdot\mathbf{B} = 0$, the transverse resistivity is $\rho_\perp = \frac{1}{\sigma_D}$. When the magnetic field is parallel to the electric current density, i.e., $\mathbf{B} \parallel \mathbf{j}$, the longitudinal resistivity is $\rho_\parallel(B) = \frac{1}{\sigma_D+\alpha B^2}$. The parameter α can then be expressed in terms of $\rho_\parallel$ and $\rho_\perp$ as $\alpha = (\rho_\parallel^{-1} - \rho_\perp^{-1})/B^2$. In practice, $\rho_\parallel$ and $\rho_\perp$ are two physical quantities to be measured experimentally. As a result, αB^2 may give rise to a negative magnetoresistivity defined as $\delta\rho_\parallel = \rho_\parallel(B) - \rho_\parallel(0)$. In addition, Eq. (1) can be explicitly derived from Eq. (4) by the vector calculation. All the parameters in Eq. (1) are measurable experimentally.

The excellent agreement between the measured AMR and PHE and that described by Eqs. (1) and (4) reveals the existence of the field-dependent current [given by Eq. (3)] in our Cd_3As_2 devices. For the Dirac semimetal Cd_3As_2, the conduction and valence bands are inverted near the Γ point to form Dirac points and the Lifshitz point, but a linear dispersion persists even when the Fermi energy E_F moves up to 250 meV above the Dirac point [26]. Since the Lifshitz energy is relatively small [34], it is believed that a strong coupling between the conduction and valence bands produces the Berry curvature, which can induce the field-dependent current according to the semiclassical theory [31,33]. If the two bands just touch at one point [35], the chiral anomaly could provide a reasonable mechanism to produce the AMR and PHE [22].

Large in-plane transverse magnetoresistance has not been well understood up to now. In this case, the effect of chiral anomaly is ruled out as the current is normal to the magnetic field. Although Abrisokov found a linear magnetoresistance at a screened Coulomb potential in the quantum limit [36], a linear magnetoresistance was observed even at relatively weak fields in many Weyl and Dirac semimetals, especially those with high mobility [37]. Therefore, the true physical mechanism is still unclear [38]. In this work, a quadratic in-plane transverse magnetoresistance is only measured in very weak fields $B < 1\mathrm{T}$ as shown in Fig. 1(d). Large positive in-plane transverse magnetoresistance clearly deviates from the quadratic behaviors when $B > 2\,\mathrm{T}$. This cannot be simply explained in the framework of the Drude theory assuming that the relaxation time is independent of field. However, the observed large magnetoresistance indicates that the relaxation time has a large correction in a finite magnetic field. Negative longitudinal magnetoresistance has been discussed in the previous paper [8]. It is worth noting that negative magnetoresistance can be also induced by some mechanisms other than chiral anomaly [31,33,39–43]. Whether these mechanisms can also induce the AMR and PHE is still an open question and deserves further study.

To conclude, we have observed giant and negative anisotropic magnetoresistance and the planar Hall effect in nonmagnetic Cd_3As_2 microribbons. Our experimental results are in excellent agreement with the theoretical descriptions and formulas of AMR and PHE. The puzzle of the angle narrowing effect which was first observed in Na_3Bi is also resolved according to the theory of AMR and PHE. Therefore, our work not only reveals unusual physical phenomena in Weyl and Dirac semimetals, but also finds additional transport signatures of Weyl and Dirac fermions other than negative magnetoresistance. The observed giant AMR and PHE in topological semimetals might also have potential applications in magnetic sensors.

Recently, we became aware of a work on the measurement of the planar Hall effect by Wu *et al.* [44].

This work was supported in part by the Research Grants Council of the Hong Kong Special Administrative Region in China under Grants No. 16305215, No. 17301116, No. C6026-16W, and No. AoE/P-04/08, and in part by the National Natural Science Foundation of China (No. 11574129) and the Natural Science Foundation of Guangdong Province (No. 2015A030313840). The electron-beam lithography facility is supported by the Raith-HKUST Nanotechnology Laboratory at MCPF.

H.L. and H.-W.W. contributed equally to this work.

[1] T. McGuire and R. Potter, Anisotropic magnetoresistance in ferromagnetic 3d alloys, IEEE Trans. Magn. **11**, 1018 (1975).

[2] J. P. Pan, in *Solid State Physics*, edited by F. Seitz and D. Turnbull (Academic, New York, 1957), Vol. 5, pp. 1–96.

[3] H. X. Tang, R. K. Kawakami, D. D. Awschalom, and M. L. Roukes, Giant Planar Hall Effect in Epitaxial (Ga,Mn)As Devices, Phys. Rev. Lett. **90**, 107201 (2003).

[4] S. Kokado, M. Tsunoda, K. Harigaya, and A. Sakuma, Anisotropic magnetoresistance effects in Fe, Co, Ni, Fe_4N, and half-metallic ferromagnet: A systematic analysis, J. Phys. Soc. Jpn. **81**, 024705 (2012).

[5] H.-J. Kim, K.-S. Kim, J.-F. Wang, M. Sasaki, N. Satoh, A. Ohnishi, M. Kitaura, M. Yang, and L. Li, Dirac versus Weyl Fermions in Topological Insulators: Adler-Bell-Jackiw Anomaly in Transport Phenomena, Phys. Rev. Lett. **111**, 246603 (2013).

[6] J. Xiong, S. K. Kushwaha, T. Liang, J. W. Krizan, M. Hirschberger, W. Wang, R. J. Cava, and N. P. Ong, Evidence for the chiral anomaly in the Dirac semimetal Na_3Bi, Science **350**, 413 (2015).

[7] X. Huang, L. Zhao, Y. Long, P. Wang, D. Chen, Z. Yang, H. Liang, M. Xue, H. Weng, Z. Fang, X. Dai, and G. Chen, Observation of the Chiral-Anomaly-Induced Negative Magnetoresistance in 3D Weyl Semimetal TaAs, Phys. Rev. X **5**, 031023 (2015).

[8] H. Li, H. He, H. Z. Lu, H. Zhang, H. Liu, R. Ma, Z. Fan, S. Q. Shen, and J. Wang, Negative magnetoresistance in Dirac semimetal Cd_3As_2, Nat. Commun. **7**, 10301 (2016).

[9] Q. Li, D. E. Kharzeev, C. Zhang, Y. Huang, I. Pletikosic, A. V. Fedorov, R. D. Zhong, J. A. Schneeloch, G. D. Gu, and T. Valla, Chiral magnetic effect in $ZrTe_5$, Nat. Phys. **12**, 550 (2016).

[10] C. L. Zhang, S. Y. Xu, I. Belopolski, Z. Yuan, Z. Lin, B. Tong, G. Bian, N. Alidoust, C. C. Lee, S. M. Huang, T. R. Chang, G. Chang, C. H. Hsu, H. T. Jeng, N. Madhab, S. Daniel, H. Zheng, J. Wang, H. Lin, C. Zhang *et al.*, Signatures of the Adler-Bell-Jackiw chiral anomaly in a Weyl fermion semimetal, Nat. Commun. **7**, 10735 (2016).

[11] C. Z. Li, L. X. Wang, H. Liu, J. Wang, Z. M. Liao, and D. P. Yu, Giant negative magnetoresistance induced by the chiral anomaly in individual Cd_3As_2 nanowires, Nat. Commun. **6**, 10137 (2015).

[12] C. Zhang, E. Zhang, W. Wang, Y. Liu, Z. G. Chen, S. Lu, S. Liang, J. Cao, X. Yuan, L. Tang, Q. Li, C. Zhou, T. Gu, Y. Wu, J. Zou, and F. Xiu, Room-temperature chiral charge pumping in Dirac semimetals, Nat. Commun. **8**, 13741 (2017).

[13] C. Shekhar, A. K. Nayak, Y. Sun, M. Schmidt, M. Nicklas, I. Leermakers, U. Zeitler, Y. Skourski, J. Wosnitza, Z. Liu, Y. Chen, W. Schnelle, H. Borrmann, Y. Grin, C. Felser, and B. Yan, Extremely large magnetoresistance and ultrahigh mobility in the topological Weyl semimetal candidate NbP, Nat. Phys. **11**, 645 (2015).

[14] A. Narayanan, M. D. Watson, S. F. Blake, N. Bruyant, L. Drigo, Y. L. Chen, D. Prabhakaran, B. Yan, C. Felser, T. Kong, P. C. Canfield, and A. I. Coldea, Linear Magnetoresistance Caused by Mobility Fluctuations in n-Doped Cd_3As_2, Phys. Rev. Lett. **114**, 117201 (2015).

[15] M. Novak, S. Sasaki, K. Segawa, and Y. Ando, Large linear magnetoresistance in the Dirac semimetal TlBiSSe, Phys. Rev. B **91**, 041203(R) (2015).

[16] R. Singha, A. K. Pariari, B. Satpati, and P. Mandal, Large nonsaturating magnetoresistance and signature of nondegenerate Dirac nodes in ZrSiS, Proc. Natl. Acad. Sci. USA **114**, 2468 (2017).

[17] H. B. Nielsen and M. Ninomiya, The Adler-Bell-Jackiw anomaly and Weyl fermions in a crystal, Phys. Lett. B **130**, 389 (1983).

[18] D. T. Son and B. Z. Spivak, Chiral anomaly and classical negative magnetoresistance of Weyl metals, Phys. Rev. B **88**, 104412 (2013).

[19] A. A. Burkov, Chiral anomaly and transport in Weyl metals, J. Phys.: Condens. Matter **27**, 113201 (2015).

[20] A. A. Burkov, Chiral Anomaly and Diffusive Magnetotransport in Weyl Metals, Phys. Rev. Lett. **113**, 247203 (2014).

[21] A. A. Burkov, Giant planar Hall effect in topological metals, Phys. Rev. B **96**, 041110 (2017).

[22] S. Nandy, G. Sharma, A. Taraphder, and S. Tewari, Chiral Anomaly as the Origin of the Planar Hall Effect in Weyl Semimetals, Phys. Rev. Lett. **119**, 176804 (2017).

[23] J. Wang, H. Li, C. Chang, K. He, J. S. Lee, H. Lu, Y. Sun, X. C. Ma, N. Samarth, S. Q. Shen, Q. K. Xue, M. H. Xie, and M. H. W. Chan, Anomalous anisotropic magnetoresistance in topological insulator films, Nano Res. **5**, 739 (2012).

[24] A. Sulaev, M. Zeng, S. Q. Shen, S. K. Cho, W. G. Zhu, Y. P. Feng, S. V. Eremeev, Y. Kawazoe, L. Shen, and L. Wang, Electrically tunable in-plane anisotropic magnetoresistance in topological $BiSbTeSe_2$ nanodevice, Nano Lett. **15**, 2061 (2015).

[25] A. A. Taskin, H. F. Legg, F. Yang, S. Sasaki, Y. Kanai, K. Matsumoto, A. Rosch, and Y. Ando, Planar Hall effect from the surface of topological insulators, Nat. Commun. **8**, 1340 (2017).

[26] Z. K. Liu, J. Jiang, B. Zhou, Z. J. Wang, Y. Zhang, H. M. Weng, D. Prabhakaran, S.-K. Mo, H. Peng, P. Dudin, T. Kim, M. Hoesch, Z. Fang, X. Dai, Z. X. Shen, D. L. Feng, Z. Hussain, and Y. L. Chen, A stable three-dimensional topological Dirac semimetal, Nat. Mater. **13**, 677 (2014).

[27] See Supplemental Material at http://link.aps.org/supplemental/10.1103/PhysRevB.97.201110 for details of the magnetoresistance (MR) and ordinary Hall resistances, in-plane AMR and PHE behaviors of another typical Cd_3As_2 ribbon device, and the **B** dependence of AMR and PHE in our Cd_3As_2 devices, which includes Refs. [8,22,26,31].

[28] K. Fujikawa and H. Suzuki, *Path Integrals and Quantum Anomalies* (Oxford University Press, Oxford, UK, 2004).

[29] K. Fukushima, D. E. Kharzeev, and H. J. Warringa, Chiral magnetic effect, Phys. Rev. D **78**, 074033 (2008).

[30] H. Z. Lu, S. B. Zhang, and S. Q. Shen, High-field magnetoconductivity of topological semimetals with short-range potential, Phys. Rev. B **92**, 045203 (2015).

[31] Y. Gao, S. A. Yang, and Q. Niu, Intrinsic relative magnetoconductivity of nonmagnetic metals, Phys. Rev. B **95**, 165135 (2017).

[32] L. Onsager, Reciprocal relations in irreversible processes. I., Phys. Rev. **37**, 405 (1931)

[33] A. V. Andreev and B. Z. Spivak, Longitudinal Negative Magnetoresistance and Magnetotransport Phenomena in Conventional and Topological Conductors, Phys. Rev. Lett. **120**, 026601 (2018).

[34] S. Jeon, B. B. Zhou, A. Gyenis, B. E. Feldman, I. Kimchi, A. C. Potter, Q. D. Gibson, R. J. Cava, A. Vishwanath, and A. Yazdani, Landau quantization and quasiparticle interference in

the three-dimensional Dirac semimetal Cd_3As_2, Nat. Mater. **13**, 851 (2014).

[35] Z. Wang, H. Weng, Q. Wu, X. Dai, and Z. Fang, Three-dimensional Dirac semimetal and quantum transport in Cd_3As_2, Phys. Rev. B **88**, 125427 (2013).

[36] A. A. Abrikosov, Quantum magnetoresistance, Phys. Rev. B **58**, 2788 (1998).

[37] T. Liang, Q. Gibson, M. N. Ali, M. Liu, R. J. Cava, and N. P. Ong, Ultrahigh mobility and giant magnetoresistance in the Dirac semimetal Cd_3As_2, Nat. Mater. **14**, 280 (2015).

[38] H. Z. Lu and S. Q. Shen, Quantum transport in topological semimetals under magnetic fields, Front. Phys. **12**, 127201 (2017).

[39] M. C. Chang and M. F. Yang, Chiral magnetic effect in the absence of Weyl node, Phys. Rev. B **92**, 205201 (2015).

[40] R. D. Reis, M. Ajeesh, N. Kumar, F. Arnold, C. Shekhar, M. Naumann, M. Schmidt, M. Nicklas, and E. Hassinger, On the search for the chiral anomaly in Weyl semimetals: The negative longitudinal magnetoresistance, New J. Phys. **18**, 085006 (2016).

[41] T. Schumann, M. Goyal, D. A. Kealhofer, and S. Stemmer, Negative magnetoresistance due to conductivity fluctuations in films of the topological semimetal Cd_3As_2, Phys. Rev. B **95**, 241113(R) (2017).

[42] X. Dai, Z. Z. Du, and H. Z. Lu, Negative Magnetoresistance without Chiral Anomaly in Topological Insulators, Phys. Rev. Lett. **119**, 166601 (2017).

[43] B. Assaf, T. Phuphachong, E. Kampert, V. Volobuev, P. Mandal, J. Sanchez-Barriga, O. Rader, G. Bauer, G. Springholz, L. de Vaulchier, and Y. Guldner, Negative Longitudinal Magnetoresistance from the Anomalous $N = 0$ Landau Level in Topological Materials, Phys. Rev. Lett. **119**, 106602 (2017).

[44] M. Wu, G. Zheng, W. Chu, W. Gao, H. Zhang, J. Lu, Y. Han, J. Yang, H. Du, W. Ning, Y. Zhang, and M. Tian, Probing the chiral anomaly by planar Hall effect in three-dimensional Dirac semimetal Cd_3As_2 nanoplates, arXiv:1710.01855.